Tutors

Dr. Francesc Mas Pujadas
Departament de Ciència de Materials i Química Física

Dr. Sergio Madurga Díez
Departament de Ciència de Materials i Química Física

Grau de Química

Treball Final de Grau

Computational study of charge regulation effect on the stretching of weak polyelectrolytes.

Estudi computacional de l'efecte de regulació de càrrega en l'estirament de polielectròlits febles.

Javier Orradre Altabás

June 2020

Universitat de Barcelona

B:KC Barcelona Knowledge Campus
Campus d'Excel·lència Internacional

If I have seen further, it is by standing on the shoulders of Giants.

Isaac Newton

I would like to express my deep gratitude to my research supervisors, Dr. Francesc Mas and Dr. Sergio Madurga, for their advice and assistance and their invaluable support throughout this project. I am extremely grateful as well to Mr. Pablo Blanco for his total dedication in the follow-up of this work, striving day by day to help me overcome the challenges of this research. It has been a great privilege and honour to work and study under their guidance.

I would also like to thank my parents and friends for providing me with the necessary moral support during this long journey. However, my special thanks go to my mother, for being the best reference I could have never dreamt of.

REPORT

CONTENTS

1. SUMMARY

Weak polyelectrolytes stretching is a flourishing research field due to the constant upgrade in the single molecule experimental techniques and the interest that the understanding of these macromolecules' behaviour awakes. For this reason, the main objective in this work is to perform a computational study about weak polyelectrolytes that allows to evaluate which relationship exists between charge regulation and mechanical stretching. In this particular case, hyaluronic acid has been chosen as the molecule of study, a natural polymer with a wide range of applications, specially in medicine and cosmetics.

This computational study is based on the implementation of a minimal theoretical model that includes the fundamental aspects that describe weak linear polyelectrolytes stretching, which are: conformational equilibrium, proton binding, bond stretching and bending, steric hinderance and mechanical work. As the analytic resolution of the model is of high complexity, it was decided that Semi-Grand Canonical MonteCarlo simulations will be used. These simulations were carried out at different pH, ionic strength and pulling force values, the latter being only employed in stretching experiments. Data obtained through simulations provides information on both conformational properties (end-to-end distance $\langle r^2 \rangle$, chain elongation L_z, persistence length l_p and Kuhn length l_k) and protonation properties (degree of protonation or coverage θ, effective acidity pK_a^{eff} and proton binding capacity C) but, above all, it provides information of the mechanisms that interrelate these properties, which are crucial to understand how charge regulation works.

Finally, a comparison is performed between the two outlines proposed to represent the hyaluronic acid macromolecule, and the differences are discussed. At the same time, while studying their behaviours, the different observed force regimes are analysed and their impact to the polyelectrolyte properties is also assessed.

Keywords: weak polyelectrolytes, coarse-grained model, MonteCarlo simulation, mechanical stretching, charge regulation, hyaluronic acid.

2. RESUM

L'estirament de polielectròlits febles és un àmbit de recerca en auge degut a la millora constant de les tècniques experimentals a nivell d'una sola molècula i a l'interès que desperta entendre el comportament d'aquestes macromolècules. Per aquest motiu, el principal objectiu d'aquest treball és la realització d'un estudi computacional sobre els polielectròlits febles que permeti avaluar quina relació existeix entre la regulació de la càrrega i l'estirament mecànic. En aquest cas, s'ha escollit l'àcid hialurònic com a molècula d'estudi, un polímer natural amb múltiples aplicacions, especialment al camp de la medicina i la cosmètica.

Aquest estudi computacional es basa en la implementació d'un model teòric minimalista que inclou els aspectes més fonamentals per descriure l'estirament de polielectròlits lineals febles com són ara: l'equilibri conformacional, la unió de protons, els moviments d'estirament i flexió dels enllaços, la repulsió estèrica i el treball mecànic. Com la resolució analítica del model és d'una elevada complexitat, es va decidir fer ús de simulacions del tipus Semi-Grand Canonical MonteCarlo a diferents valors de pH, força iònica i força de tracció, emprant l'última només en els casos dels experiments d'estirament. Les dades obtingudes mitjançant aquestes simulacions proporcionen informació tant de les propietats conformacionals (distància d'extrem a extrem $\langle r^2 \rangle$, allargament de la cadena L_z, longitud de persistència l_p i longitud de Kuhn l_k) com de les propietats de protonació (grau de protonació o recobriment θ, la constant d'acidesa efectiva pK_a^{eff} i la *binding capacity* dels protons C), però sobretot dels mecanismes que les relacionen entre elles i que són crucials per entendre com funciona la regulació de la càrrega.

Finalment es duu a terme una comparació entre dos dissenys proposats per representar la macromolècula d'àcid hialurònic i es discuteixen les seves diferències. Alhora, en estudiar els seus comportaments, s'analitzen els diferents règims de força observats i com aquests afecten a les propietats del polielectròlit.

Paraules clau: polielectròlits febles, model de gra-gruixut, simulació MonteCarlo, estirament mecànic, regulació de la càrrega, àcid hialurònic.

3. INTRODUCTION

Polyelectrolytes (PEs) have been subject of study over many years due to their ubiquitous presence both in natural sources (proteins, nucleic acids…) and in synthetic chemistry. They are described as polymers whose repeating units bear ionizable functional groups and, therefore, they display characteristics from electrolytes such as high solubility and conductivity, but also, others typical from polymers, like the tendency to form viscous solutions [1].

The aim of this project is to study the physicochemical properties of these PEs and, specially, how do they become modified when subjected to different force regimes. In order to achieve this purpose, a minimal computational model which accounts for the fundamental aspects of weak PEs stretching has been used. Nevertheless, some general background will be discussed before illustrating the model in the subsequent sections.

3.1. WEAK POLYELECTROLYTES

PEs can be categorized into two different subgroups, strong and weak ones, depending on the way their charge is modulated when they are submerged in a solution. A *strong* polyelectrolyte is considered to completely dissociate in solution at almost any pH condition whereas a *weak* polyelectrolyte has an acid dissociation constant (K_a) with values in the range of 10^{-2} to 10^{-10} [1], (although these figures may depend on the consulted source [2]) meaning that it will be partially dissociated at intermediate pHs. This specific feature of weak PEs provides the possibility to alter their degree of protonation (and therefore, other physicochemical properties of the chain) by changing the environment conditions (pH, ionic strength, force…), a phenomenon known as Charge Regulation (CR) [3].

Understanding the complex processes that lead to CR is of paramount importance to comprehend the behaviour of weak PEs in a wide range of situations. Just to mention a few cases, the handling of charge in macromolecules plays a crucial role in supramolecular chemistry [4], wastewater treatment [5] (by metal-ion complexation with the PEs), stability of colloidal systems [6] and advanced coating in material sciences (like nanoparticles protection and functionalization or formation of multilayer coatings) [7,8].

This CR processes can take place in rigid structures but, in general, weak polyelectrolytes are flexible and hence conformational and ionization degrees of freedom are energetically coupled; a fact which can generate radical structural changes in the macromolecule. For this reason, our model must precisely consider all the necessary parameters to reproduce in detail the connection between both phenomena, as it will play an elemental role in determining the relation among the physicochemical properties of the chain and the applied force when performing stretching experiments.

3.2. DESCRIPTION OF THE HYALURONIC ACID

In this work, the molecule of interest has been a high molecular weight biopolysaccharide, discovered in 1934 by K. Meyer and J. Palmer in the vitreous of bovine eyes [9], which is named hyaluronic acid (HA). It is a mucopolysaccharide (a type of carbohydrate) that occurs naturally in all living organisms, and which can be several thousands of sugars (monomers) long.

In the body, HA is commonly manifested in its salt form, hyaluronate, and it can be found in high concentrations in either extracellular or intracellular matrix of connective tissues, although it appears mostly in the first ones [10]. Some examples of these connective tissues include skin, umbilical cord, synovial fluid and vitreous humor; albeit substantial quantities have been also detected in lungs, kidney, brain and muscle tissues.

3.2.1. Chemical structure

As it was introduced before, the HA chain is formed by the union of small sugar entities (monomers) which in this specific case are disaccharides of D-glucuronic acid and D-N-acetylglucosamine, that are linked together through alternating beta-1,3 and beta-1,4 glycosidic bonds. The beta configuration of these linkages allows to maintain the bulky groups in the sterically favoured equatorial positions, while the disfavoured axial positions are occupied by the small hydrogen atoms (**Figure 1**). Thereby, the structure of the monomer is very stable from the energetic point of view.

Each disaccharide measures about 1 nm long, weighs around 400 Da and contains an ionizable carboxylic group whose intrinsic pK_a is 3.0 [12]. The linear weak polyanion (a PE which develops negative charge in solution) is formed then by joining these monomers with the hyaluronan synthase enzymes, producing chains of up to 10.000 monomers; achieving contour

lengths (L_c, distance of the PE when it is stretched from end to end) on the micron scale and molecular weights of a few million Da [13].

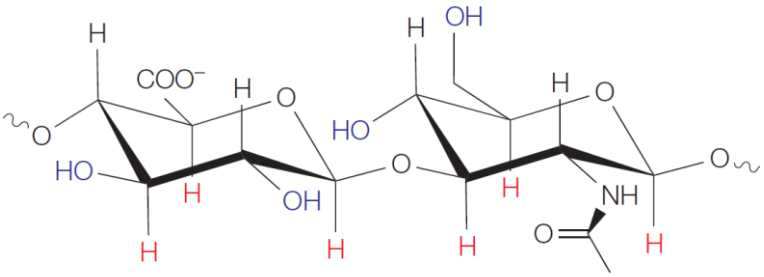

Figure 1. HA negatively charged monomer, a disaccharide with structure [(1→3)-β-d-GlcNAc-(1→4)-β-d-GlcA-] (*image extracted from Toole et al.* [11]).

3.2.2. Properties and applications

The biological properties of HA include preservation of the elastoviscosity of connective liquid tissues, lubrication of movable parts of the body (like joints and muscles), control of tissue hydration and water transport, and numerous receptor-mediated roles in cell detachment, mitosis, etc [14,15]. However, due to its consistency and tissue-friendliness, business leaders in the cosmetic sector have used HA in skin-care products as an excellent moisturizer.

On the other hand, HA has also been used the last decades in a huge number of clinical applications because of its unique viscoelastic nature and biocompatibility. For instance, as supplementation of joint fluid in arthritis and as a surgical aid in eye surgery [16,17]. More recently, HA has also been investigated as a drug delivery agent for a wide variety of administration routes [18].

3.3. THEORETICAL PREVIOUS MODELS

In order to simulate the characteristics of neutral polymer chains, some models had been developed long before now [19]. Notwithstanding, the incorporation of charge fluctuation and electrostatic interactions to accurately reproduce weak PEs made them become less precise due to the impossibility to include parameters for all those aspects.

Despite the fact that these models are not going to be used to actually describe our molecule of concern (HA), it is quite important to have a general idea about them, just to get

involved in the methodology used to represent macromolecules of such style. For this reason, a brief introduction on the *Freely Jointed Chain* (FJC) and the *Worm-Like Chain* (WLC) models is displayed below.

3.3.1. Freely Jointed Chain model

In the *Freely Jointed Chain* model, the macromolecular chain is represented at the coarse-grained level by a set of **N** rigid, linear linkages of length **b** known as Kuhn segments, which are joined together at their ends by joints with fully random orientation. One of the biggest nuisances of the FJC is that by allowing the rotation in any direction, steric hinderance (EV, excluded volume) is neglected between different monomers, and implausible configurations become permitted. Apart from that, although the model has been able to provide great results in the stretching properties of some synthetic polymers, it showed clear deviations in the elastic measurements of some polyelectrolytes such as double stranded DNA [20].

To enhance the viability of the model, some authors have tried to introduce upgrades to the FJC model like the freezing of bond angles [21] (*Freely Rotating Chain*), the subdivision of the linkages in smaller pieces to simulate a more flexible chain or the introduction of harmonic potentials to enhance the elasticity by assuming spring-like segments [22,23]. Nevertheless, these improvements are not able to walk away from the simplistic FJC model and it still has shortcomings for our purpose [24].

3.3.2 Worm-Like Chain model

The *Worm-Like Chain* model, firstly proposed by Kratky and Porod in 1949 [25], goes one step further than the FJC, being able to reproduce the intrinsic elasticity that causes many biological molecules to remain rigid at small lengths scales but significantly flexible over longer lengths. The WLC assumes that the macromolecule is inextensible, is ruled by a linear elastic bending energy and is subjected to thermal fluctuations [26]. Besides, it introduces l_p, the persistence length, whose value determines the length scale in which the PE suffers the transition from the stiff behaviour at short distances to the flexible behaviour at the span of the polymer.

$$F(z) = \frac{k_b T}{l_p}\left[\frac{1}{4}\left(1 - \frac{z}{L_c}\right)^{-2} + \frac{z}{L_c} - \frac{1}{4}\right] \quad (1)$$

The WLC can also be extended to incorporate a force along the *z*-axis in order to perform analytic stretching studies [27], that are frequently interpolated by the formula of Marko and Siggia [28] (**Equation 1**), where k_b is the Boltzmann constant and T is the temperature. Even though it shows really ameliorated results with respect to those obtained in the FJC for DNA stretching [29], the WLC model is not capable of reproducing stretching properties at high force regimes since it assumes that the PE is inextensible. Thus, as it occurs with the FJC, the WLC is not complete enough for achieving the targets of this project, although some of its theoretical aspects, like the persistence length, will be implemented.

3.4. EXPERIMENTAL METHODS

Nowadays, single-molecule force spectroscopy (SMFS) has emerged as a powerful tool to investigate forces and motions associated with biological molecules and enzymatic activity. Optical tweezers, magnetic tweezers and atomic force microscopy (AFM) stand out among the most commonly used techniques [30], although perhaps the last one is the best known of the three [24].

AFM-SMFS is ideal to complement the computational studies performed in this project since it provides the necessary stretching information to validate the methodology and is capable to conduct measurements at the required conditions. At the same time, AFM's simplicity and rapid sample preparation [30] confer it advantages over the rest of techniques, making it suitable for this particular case.

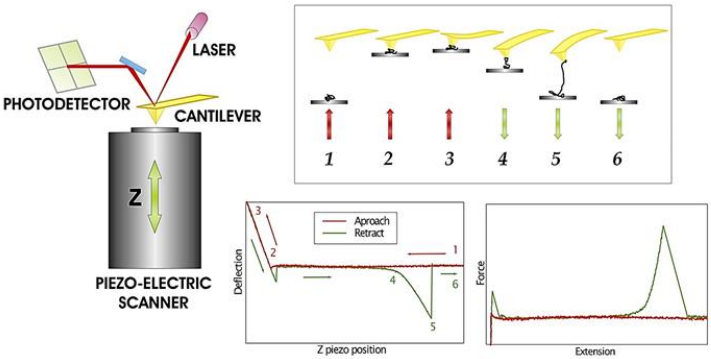

Figure 2. Scheme of an AFM-SMFS stretching experiment (*image extracted from Giannotti et al.* [19]).

The operation of the technique is schematized in **Figure 2**. Firstly, the weak PE chain is adsorbed onto a solid substrate linked to the piezoelectric, a part of the AFM instrument able to perform precise movements along the z-axis. Then, the piezoelectric is displaced towards the cantilever until it slightly deflects upwards due to contact, to ensure that the macromolecule is adsorbed onto the tip (**Figure 2**, steps 1-3). After that, the piezoelectric is moved in the opposite direction, the cantilever deflects downwards, and the molecule is stretched until it either breaks or desorbs from the points where it is attached (**Figure 2**, steps 4-6). During this process, a laser-photodetector tandem records all the deflection data that in turn is converted into force by means of the Hooke's law, being k the cantilever spring constant (**Equation 2**).

$$F(z) = -k \cdot (z - z_0) \qquad (2)$$

Combining this information with the displacement data from the piezoelectric, the force-extension curves from the polymer stretching can be graphed, and hence, compared to those provided by the simulations.

4. OBJECTIVES

The main ambition of this project is to achieve to design a model able to carefully reproduce weak polyelectrolytes stretching behaviour. In order to reach this objective, the model has to attempt to portray real AMF force-extension curves from experiments performed at different pH and ionic strength conditions while it must be computationally feasible, a fact that for now greatly restricts the use of all-atom simulations [31]. For this reason, one of the fundamental intentions is to adapt as accurately as possible the coarse-grained profile to our molecule of study (HA) by means of a correct spatial distribution of the chemical groups and a complete description of the electrostatic interactions.

The theoretical-analytic study of weak PEs is out of the scope of this work due to its high mathematical complexity, so, the correct adequation and generalisation of a previous Semi-Grand Canonical Monte Carlo (SGCMC) code from our group is also a point of paramount

importance to obtain trustable data. Furthermore, slight improvements might be needed to avoid local and statistical errors during the programme execution.

Finally, the last major target of this project is to analyse the results provided by the SGCMC simulations and draw conclusions from them; studying the variables, identifying characteristic patterns and clarifying why does the macromolecule behave that way.

5. THEORETICAL BACKGROUND

As introduced in previous sections, this study has been performed using a minimal model at the coarse-grained level that still captures the fundamental aspects present in the stretching of a weak linear polyelectrolyte: bond stretching, bond bending, internal angle rotation, proton binding and electrostatic interactions [3].

Foremost, the model will be thoroughly described so that it is understood how it works and what parameters are needed in order to depict such a macromolecule as HA, thereafter, an explanation of the chosen outlines to describe the HA weak polyelectrolyte will be presented in great detail.

5.1. MINIMAL MODEL OF A WEAK FLEXIBLE POLYELECTROLYTE

The vast majority of coarse-grained models that feature probabilistic simulations (e.g. Monte Carlo methods) to represent the stretching of weak PEs are based on calculating the energy of the macromolecule and minimizing it in order to obtain the most stable conformations by changing a certain number of allowed parameters. Therefore, the level of correspondence with reality depends on the capability of the simulation program to find those energy minima but primarily on how rigorously the model depicts the polyelectrolyte behaviour.

As a means of achieving a complete definition for the free energy of the system, the ionization state of the macromolecule has been described by a set of variables $s = \{s_i\}$ with $i = 1 \dots N$, where $s_i = 1$ indicates that the site is protonated (no charge in the HA case, since the functional group is a carboxylate), $s_i = 0$ the opposite (HA site negatively charged) and N is the total number of protonating sites. The conformational state is determined by $c = \{\phi_j\}$,

$j = 1 \dots M$, where ϕ_j is the internal rotational angle of bond j, which is assumed to be in a state associated to an energy minima (commonly *trans* (t), *gauche*+ (g^+) and *gauche*$^-$ (g^-)) since these are the ones significantly populated; and M is the total number of bonds, that can be easily related to N, although this connection will depend on the chosen outline. The assumptions made for the ionization and conformational states correspond to the Site Binding (SB) [32] and Rotational Isomeric State (RIS) [33,34] models respectively, and the combination of both two leads up to the Site Binding Rotational Isomeric State (SBRIS) model which is the cornerstone of this work [35].

In addition, to get a closer image of the PE, other contributions to the total free energy must also be taken into account, such as flexibility of bond lengths and angles, excluded volume effects, electrostatic interactions and the mechanical work derived from the applied force, which is going to be of crucial relevance in our stretching studies [36]. Hence, the free energy of the system can be expressed as

$$\mathcal{F}(s,c) = \mathcal{F}_{rot} + \mathcal{F}_p + \mathcal{F}_{length} + \mathcal{F}_{angle} + \mathcal{F}_E + \mathcal{F}_{EV} + W \qquad (3)$$

where

$$\mathcal{F}_{rot} = k_b T \sum_{j=1}^{M} \epsilon_{rot,j}(\phi_j) \qquad (4)$$

is the RIS free energy contribution that is calculated by adding up all the torsional energies $\epsilon_{rot,j}(\phi_j)$ of the M rotating bonds. As presented a few lines above, RIS approximation restricts the values of ϕ_j to π (*trans*), $+\pi/3$ (*gauche*+) and $-\pi/3$ (*gauche*$^-$) thereby enabling only three possible values for $\epsilon_{rot,j}(\phi_j)$.

The term $\mathcal{F}_p$ is related to the energy of a particular ionization state, and is defined as

$$\mathcal{F}_p = k_b T \sum_{i=1}^{N} \ln(10)\, \mu_i s_i = k_b T \sum_{i=1}^{N} \ln(10)(\mathrm{pH} - \mathrm{p}K_{a,i}) s_i \qquad (5)$$

where $\mu_i = pH - pK_{a,i}$ is the reduced chemical potential corresponding to a certain hydrogen cations potential $pH = -\log(a_{H^+})$ and the intrinsic acidity provided by the negative logarithm of the acidity constant of site i, $pK_{a,i}$ [35,37].

The labels $\mathcal{F}_{length}$ and $\mathcal{F}_{angle}$ represent the resiliency of bond length l_j and bond angle α_j through the use of harmonic potentials, that will act independently from the ionization state of the sites.

$$\mathcal{F}_{length} = \sum_{j=1}^{M} \frac{k_{length,j}}{2} \left(l_j - l_{j,0}\right)^2 \quad (6)$$

$$\mathcal{F}_{angle} = \sum_{j=1}^{M-1} \frac{k_{angle,j}}{2} \left(\alpha_j - \alpha_{j,0}\right)^2 \quad (7)$$

The values $k_{length,j}$, $k_{angle,j}$, $l_{j,0}$ and $\alpha_{j,0}$ from **Equations 6** and **7** are the bond stretching and bending force constants and the equilibrium length and angle of bond j, respectively.

The electrostatic interaction energy among charged sites $\mathcal{F}_E$ is split into specific $\mathcal{F}_{SI}$ and non-specific $\mathcal{F}_{NSI}$ interactions:

$$\mathcal{F}_E = \mathcal{F}_{SI} + \mathcal{F}_{NSI} \quad (8)$$

It is important to draw a clear distinction between both contributions due to the fundamental dissimilarities in their physical mechanism. Non-specific interactions (NSI) are reasonably well-described by simple pair-potentials since they are, just as the name suggests, chemically unspecific and mediated by the solvent. In this model the Debye-Hückel (DH) potential [3] has been selected for this purpose

$$\mathcal{F}_{NSI} = k_b T \sum_{i=1}^{N} \sum_{j=i+2}^{N} \frac{l_B}{d_{ij}} e^{-\kappa d_{ij}} q_i q_j \quad (9)$$

where d_{ij} is the distance between sites i and j, $q_{i/j}$ are the charges at a certain deprotonating site i or j and can be defined as $q_{i/j} = s_{i/j} - 1$, and parameters $l_B = e^2/4\pi\varepsilon k_B T \sim 0.7$ nm and $\kappa^{-1}(\text{nm}) = 0.304/\sqrt{I\ (\text{M})}$ are the Bjerrum and the Debye lengths in water at 298.15 K and ionic strength I. Remember that the Bjerrum length is defined as the distance at which the interaction between two elementary charges is comparable in magnitude to the thermal energy ($k_B T$) and that the Debye length indicates the scale over which mobile charge carriers (ions in solution in this case) screen out the electric fields generated by a certain charge or conductor.

On the other hand, specific interactions (SI) are mediated by the backbone of the macromolecule and, consequently, it does exist a strong dependence on the chemical environment of the interacting sites that is parameterized as follows

$$\mathcal{F}_{SI} = k_b T \ln(10) \sum_{i=1}^{N-1} \epsilon_{int,i\leftrightarrow i+1}(c) s_i s_{i+1} \quad (10)$$

where $\epsilon_{int,i\leftrightarrow i+1}(c)$ corresponds to the interaction energy between sites i and i+1, which are joined by a certain configuration of bonds j, given a conformational state $c = \{\phi_j\}$ [36]. Note that, if there was enough computational capability to include doublet, triplet interactions and so on until the N-1 protonating sites, NSI could be treated as SI, providing a method (the so-called cluster expansion [37–39]) to entirely include all electrostatic contributions.

The steric EV effects $\mathcal{F}_{EV}$ to consider the finite size of the elements that compose the chain of the weak PE will be implemented by means of a hard-sphere potential (**Equation 11**) [36], which prevents the centres of two chemical groups (with radius of gyration R_k and R_l) from approaching less than a distance d_{kl} equal to the sum of both radius. When EV effects are switched off, all chemical groups are treated as points ($R_k = 0 \; \forall \; k$).

$$\mathcal{F}_{EV} = \sum_{k,l=k+4}^{M+1} \begin{cases} \infty \; ; \; d_{kl} \leq R_k + R_l \\ 0 \; ; \; d_{kl} \geq R_k + R_l \end{cases} \tag{11}$$

Finally, the mechanical work W exerted by the applied force $\boldsymbol{F}$ that is used to analyse the stretching properties of the weak PE is quantified as

$$W = -\boldsymbol{F} \cdot \boldsymbol{r} \tag{12}$$

where $\boldsymbol{r}$ is the end to end vector of the macromolecule, calculated by subtracting the position of the first chemical group ($\boldsymbol{r}_1$) to the last one of the chain ($\boldsymbol{r}_{M+1}$) [3,36].

5.2. HYALURONIC ACID OUTLINES

This minimal model was designed to be used with linear PEs and, since the HA molecule contains rings and relatively large substituents (see **Figure 1**), the first decision to be made was to accord which arrangement would be the most suitable without breaching the linearity requirements of the programme. Around this prerequisite two different distributions were proposed, being one of the two more sophisticated than the other, just to determine which level of coarse-graining was needed to faithfully reproduce the PE characteristics.

5.2.1. Description of the HA-CG4 outline

In this representation, which was firstly conceived at [40], the HA chain is considered symmetric (i.e. the chain has a plane of symmetry when it is completely elongated), thus avoiding tacticity drawbacks. Each monomer is represented with four spheres linked together

one after the other, that stand for both HA rings and the oxygens joining them, as shown in **Figure 3**.

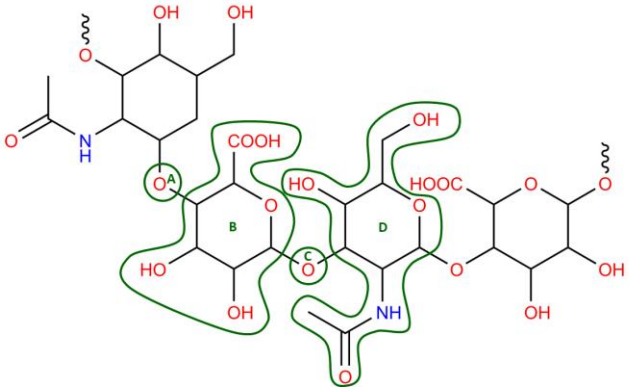

Figure 3. HA-CG4 outline.

In the scheme, group B illustrates the ring which contains the ionizable site, which can adopt two possible states: protonated (uncharged) or deprotonated (charged), imitating the hydrogen equilibria of carboxylic acid; whereas chemical groups A, C and D simulate the rest of the chain as inert sites. Bond distances and angles are considered flexible and governed by harmonic potentials as it has been explained in the previous section, but internal angle rotation is only allowed between different monomers and not within the disaccharide. Furthermore, SI are neglected due to the large distance (and therefore low correlation) between adjacent protonating sites, and only NSI mediated by the solvent and described by the DH potential are considered. The parameters chosen to describe the spatial configuration in this outline are detailed in **Table 1**.

Table 1. This table shows the parameters used to describe HA-CG4 (radii of gyration R_n, equilibrium bond distances $d_{n,n+1}$, equilibrium bond angles $\alpha_{n,n+1,n+2}$, and internal rotational angles $\phi_{n,n+1,n+2,n+3}$), where n is the chemical group of a certain row, and $n+a$ the chemical group a rows further. Note that internal rotational angles marked with a star will be able to rotate taking values of 180º, 60º and -60º.

C.G. (n)	R_n	$l_{n,n+1}$	$\alpha_{n,n+1,n+2}$	$\phi_{n,n+1,n+2,n+3}$
A	1.0	2.81	162.2	-167.60
B	4.1	2.81	150.0	-55.80
C	1.0	2.86	122.2	-119.70*
D	4.7	2.86	110.0	-78.70

5.2.2. Description of the HA-CG9 outline

In this new and more itemised layout, each disaccharide of the HA molecule is considered to be formed by 9 linearly joined spheres which simulate the chemical groups drafted in **Figure 4**. In order to simplify, the chain is assumed to be isotactic, which signifies that the stereochemistry of each monomer would be exactly reproduced without alterations along the macromolecule.

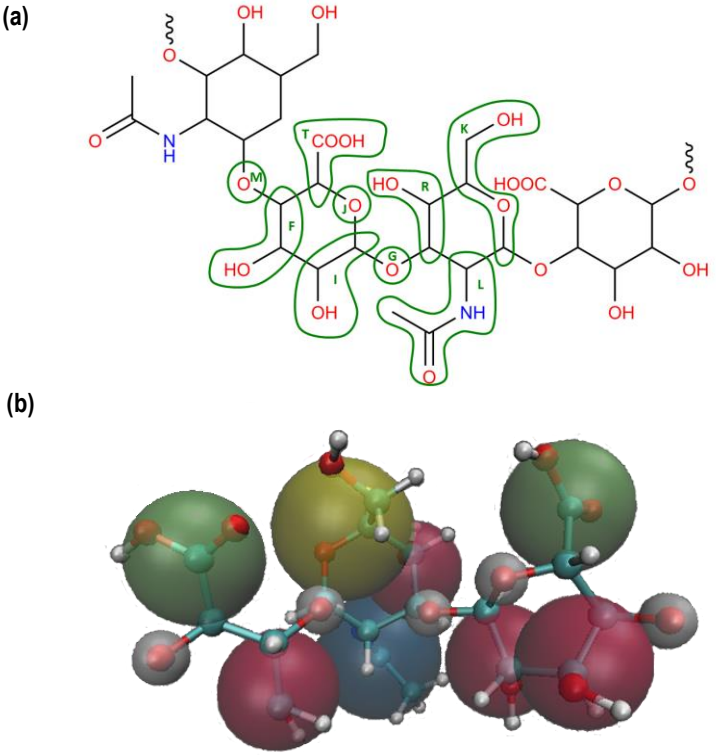

Figure 4. (a) HA-CG9 outline and (b) superposition of the HA-CG9 outline with the actual HA molecule monomer.

Now, the ionizable site is reduced to chemical group T, which does not include the whole first chemical ring anymore but almost only the carboxylic acid, thereby delimiting more accurately the deprotonation region. The rest of the groups are treated as inert sites, and the overall structure of the weak PE can be assembled by means of the data displayed in **Table 2**. Bond distances and angles are considered flexible around a certain equilibrium value as in the

first outline, although in this instance, internal angle rotation within the monomer is also allowed through the oxygens connecting the chemical rings. Electrostatic SI are turned off because of the scarce correlation between ionizable sites and solely NSI are considered through the DH potential.

Table 2. This table shows the parameters used to describe HA-CG9 (radii of gyration R_n, equilibrium bond distances $d_{n,n+1}$, equilibrium bond angles $\alpha_{n,n+1,n+2}$, and internal rotational angles $\phi_{n,n+1,n+2,n+3}$), where n is the chemical group of a certain row, and $n+a$ the chemical group a rows further. Note that internal rotational angles marked with a star will be able to rotate taking values of 180º, 60º and -60º.

C.G. (n)	R_n	$l_{n,n+1}$	$\alpha_{n,n+1,n+2}$	$\phi_{n,n+1,n+2,n+3}$
M	0.60	2.05	67.13	-167.60
F	1.48	3.64	43.99	-55.80
T	1.53	2.38	112.27	-119.70
J	0.60	2.53	57.43	114.70*
I	1.44	2.23	109.95	78.30*
G	0.60	2.57	90.98	69.70
R	1.44	3.08	32.80	-134.70
L	1.84	4.80	67.29	-51.50*
K	1.98	2.29	151.64	-78.70*

6. COMPUTATIONAL DETAILS

6.1. SEMI-GRAND CANONICAL MONTECARLO CODE

The minimal model proposed in the previous section is analysed by means of simulations with the Semi-Grand Canonical Monte Carlo (SGCMC) methodology in order to study the variations of the HA physicochemical properties; setting the pH, force and ionic strength values as the control variables, keeping them constant during the computation.

To conduct these simulations on the SGCMC code all initial and equilibrium data from the selected HA model (**Table 1** or **2** depending on the case) must be entered first. Then, the length

of the chain is introduced into the program in terms of the $(M+1)$ chemical groups, which in this work is set to the value of 81 (HA-CG4) and 181 (HA-CG9) to obtain a total of $N = 20$ ionizable sites, since through various experiments this size has been proven to provide good reproducibility of the PE intensive properties, but without originating excessive computational costs. Other important parameters that must be specified are: the periodicity of the chemical groups; the intrinsic acidity constant of each deprotonating site, fixed at the value of 10^{-3} (pK_a = 3.0); and the stretching and bending constants that, in order to simplify, have been established for all bond lengths and angles as 300 Kcal·mol^{-1}·A^{-2} (for both HA-CG4 and HA-CG9) and 0.01 Kcal·mol^{-1}·deg^{-2} (for HA-CG4) or 1 Kcal·mol^{-1}·deg^{-2} (for HA-CG9, to avoid ring deformation) respectively.

Afterwards, the relative probability of the internal rotational angle states must be established. To streamline the process, *trans* (t), *gauche*+ (g^+) and *gauche*$^-$ (g^-) states are considered equiprobable, and the preference of some conformations over the others is relegated to electrostatic and excluded volume effects. With respect to the electrostatic contributions, since SI are switched off, the only remaining interplay between the carboxylate groups will be the NSI mediated by the solvent via the DH potential.

As a means to generate new random states an adapted version of the Metropolis-Hastings algorithm has been assumed [41]. This methodology allows to draw samples from a probability distribution $p(x)$, from which direct sampling is complicated, provided that we know a function $f(x)$ whose values can be calculated and that is proportional to $p(x)$. In this case $f(x)$ is chosen as

$$f(x) = \frac{e^{-\frac{\mathcal{F}(s,c)}{k_b T}}}{Z} \tag{13}$$

where Z represents the partition function of the system, which is used to normalise $f(x)$, and $\mathcal{F}(s,c)$ the free energy of a certain configuration, computed according to **Equation 3**.

The Metropolis algorithm is an iterative process. It is initialized by selecting an arbitrary configuration with free energy $\mathcal{F}(s_0, c_0)$ which will be equated to $\mathcal{F}(s_t, c_t)$ for the first step. Thereafter, each iteration t (also named MonteCarlo step), with initial value $\mathcal{F}(s_t, c_t)$, will generate a new configuration with energy $\mathcal{F}(s', c')$, by changing the parameters depicted of the minimal model, following the outline from **Figure 5**.

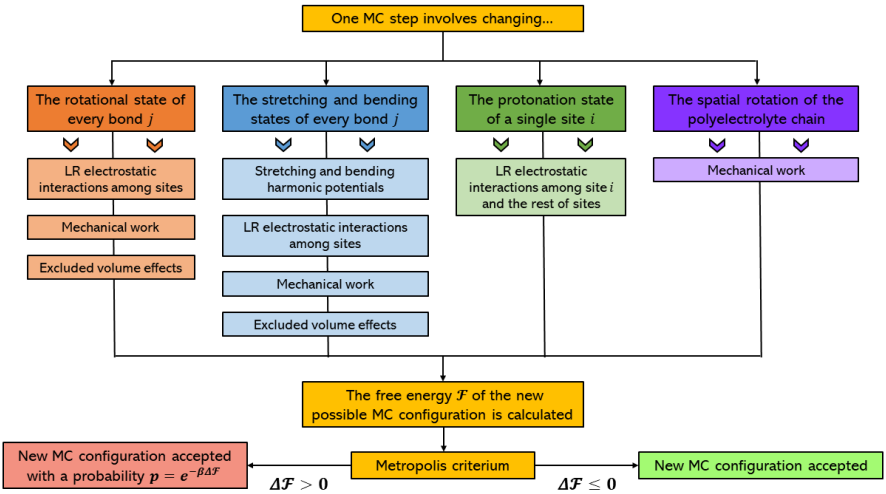

Figure 5. Layout indicating how to obtain a new MC configuration.

To determine whether the current state is feasible or not, the total free energy of the new chain $\mathcal{F}(s', c')$ is compared to that of the previous configuration, $\mathcal{F}(s_t, c_t)$. For that purpose, an acceptance ratio α is defined as

$$\alpha = \frac{f\left(\mathcal{F}(s', c')\right)}{f\left(\mathcal{F}(s_t, c_t)\right)} = \frac{e^{-\frac{\mathcal{F}(s\prime, c\prime)}{k_b T}}}{e^{-\frac{\mathcal{F}(s_t, c_t)}{k_b T}}} = e^{-\frac{\mathcal{F}(s\prime, c\prime)}{k_b T} - \left(-\frac{\mathcal{F}(s_t, c_t)}{k_b T}\right)} = e^{-\frac{\Delta\mathcal{F}}{k_b T}} \qquad (14)$$

where $\Delta\mathcal{F} = \mathcal{F}(s', c') - \mathcal{F}(s_t, c_t)$ is the free energy difference between the proposed and the previous configuration. Then,

- If $\alpha \geq 1$, which means that $\Delta\mathcal{F} \leq 0$, the new MC configuration is directly accepted since it has a lower (or at least equal) free energy than the previous one, and therefore $\mathcal{F}(s_{t+1}, c_{t+1})$ becomes $\mathcal{F}(s', c')$.
- If $0 < \alpha < 1$, which is to say that $\Delta\mathcal{F} > 0$, either the value is accepted with probability α and $\mathcal{F}(s_{t+1}, c_{t+1}) = \mathcal{F}(s', c')$; or it is rejected with probability $1 - \alpha$ and $\mathcal{F}(s_{t+1}, c_{t+1})$ becomes $\mathcal{F}(s_t, c_t)$ again instead.

In order to maintain the acceptance ratio near to its optimal value around 20% [42,43], the MC code constantly adapts the variable's differentials, enabling to explore more conformational options and reducing the chances of getting trapped in an energy minimum.

6.2. ACQUISITION OF THE HYALURONIC ACID PROPERTIES

To obtain the physicochemical properties of the HA chain, simulations are divided into two sub-processes: the equilibration process and the measurement process. The first one is designed to bring the chain from its initial state provided by the entered data to another one more stable, given some pH, force and ionic strength conditions imposed for each particular experiment. It consists of a total of 50.000 MC steps and no data is extracted from it. The second one, however, already starts from the equilibrium state found in the first process and, over its 100.000 MC steps duration, collects all the data that will be used to compute the polymer properties. Hereafter, the way in which the HA features have been determined is explained in detail.

The subsequent equation shows how the average degree of protonation θ is computed:

$$\theta = \frac{\langle N_p \rangle}{N} \tag{15}$$

where $\langle N_p \rangle$ is the thermal average of protonated sites throughout the PE chain. Inasmuch as the simulations are performed at constant pH, $\langle N_p \rangle$ will vary among the different configurations but will remain stable around a certain equilibrium value. Moreover, from the degree of protonation another interesting attribute of the polymer can be obtained, which is the effective acidity constant K_a^{eff}, that indicates how the HA deprotonation equilibrium behaves at the macroscale level (**Equation 16**), where $R-AH$ represents the weak PE ionizable sites binded to protons, $R-A^-$ the sites negatively charged and $H^+$the protons in solution.

$$R-AH \rightleftharpoons R-A^- + H^+ \tag{16}$$

$$pK_a^{eff} = pH + log\left(\frac{\theta}{1-\theta}\right) \tag{17}$$

Normally, to work with more enlightening figures, pK_a^{eff} is used instead of K_a^{eff}, and it is calculated directly from **Equation 17**. Note that this parameter is effective and only indicates how the PE would behave at certain external conditions, since actual equilibrium takes place at each site i of the chain and is not an overall mechanism [3].

In order to analyse the behaviour of the previous relations, it is useful to define the binding capacity (**Equation 18**), an amount that is used to quantify the average fluctuation of protons binding to the ionizable sites of the macromolecule [36,44].

$$C = \langle \left(N_p - N\theta\right)^2 \rangle = N \left(\frac{\partial \theta}{\partial \mu}\right)_F \tag{18}$$

An important characteristic is that binding capacity maxima appear at the pH value that corresponds to the inflection point of the coverage titration curve.

The mean squared distance of the polymer chain (**Equation 19**) is found by subtracting the vector position of the first chemical group of the polymer to that of the last chemical group, and then squaring the resulting value. Similarly, the projection of the average extension of the PE chain in the direction of the mechanical force, which is considered the z-axis, can also be obtained as shown in **Equation 20**, where z_1 is the z-coordinate of the first coarse-grained group of the chain and z_{M+1} is the z-coordinate of the last one.

$$\langle r^2 \rangle = \langle |r_{M+1} - r_1|^2 \rangle \tag{19}$$

$$L_z = \langle z_{M+1} - z_1 \rangle \tag{20}$$

Another striking parameter to evaluate is the Kuhn length [45], which represents how long each chain fragment would be if the PE was considered with the FJC model. As it is not possible to predict how many fragments would form this ideal FJC, the following expression for the mean squared distance can be rearranged thanks to the definition of the contour length (L_c) in terms of the average ring length l_r, and thus the Kuhn length value is calculated as

$$\langle r^2 \rangle = N_{frag} {l_k}^2 = L_c l_k = 2N l_r l_k \tag{21}$$

$$l_k = \frac{\langle r^2 \rangle}{2N l_r} \tag{22}$$

where l_r is found by establishing the equilibrium distance of both HA rings among the binding oxygens and taking an average of the two, N_{frag} would be the fragments forming the chain if it

was treated as a FJC, and L_c is considered to be the chain fully extended (with angles between rings of 180º).

Lastly, one more practical quantity to characterize the PE stretching mechanism is the persistence length, l_p. This parameter, introduced with the WLC model in this text, provides a length scale in which distances within the chain that are below l_p are considered stiff, and those above l_p are seen as flexible; although it can also be interpreted as the transition value above which the polymer is regarded to be not correlated. There are several methods to compute l_p [25,46], albeit in this study it has been decided to use an adapted expression that considers a chain formed by stiff segments of distance l_r [3].

$$l_p = \frac{\langle r^2 \rangle}{4Nl_r} + \frac{l_r}{2} = \frac{1}{2}(l_k + l_r) \tag{23}$$

As a result, if these equations are examined for the ideal FJC model, the Kuhn length becomes equal to the average ring length $\left(l_k^{FJC} = l_r\right)$ and the persistence length equates to the other two as well $\left(l_p^{FJC} = l_k^{FJC} = l_r\right)$.

7. RESULTS AND DISCUSSION

In this section, all data extracted from the HA simulations is analysed meticulously with the purpose of determining the effect of each control variable on the macromolecule properties. The influence of the variables during the titration and stretching experiments is explained using the HA-CG9 outline since it is the most complete of the two, however, a comparison between both layouts is displayed at the end to ascertain which differences arise.

7.1. EXPERIMENTS AT ZERO-FORCE

In the first place, the HA behaviour is studied without exerting any mechanical force, in order to evaluate the coupling of conformational and ionization degrees of freedom when no external work contributes to the free energy. To do so, the quantities introduced in section 6 have been represented in **Figures 6** and **7** as titrations curves at four distinct ionic strengths (1M, 0.1M, 0.01M and 0.001M).

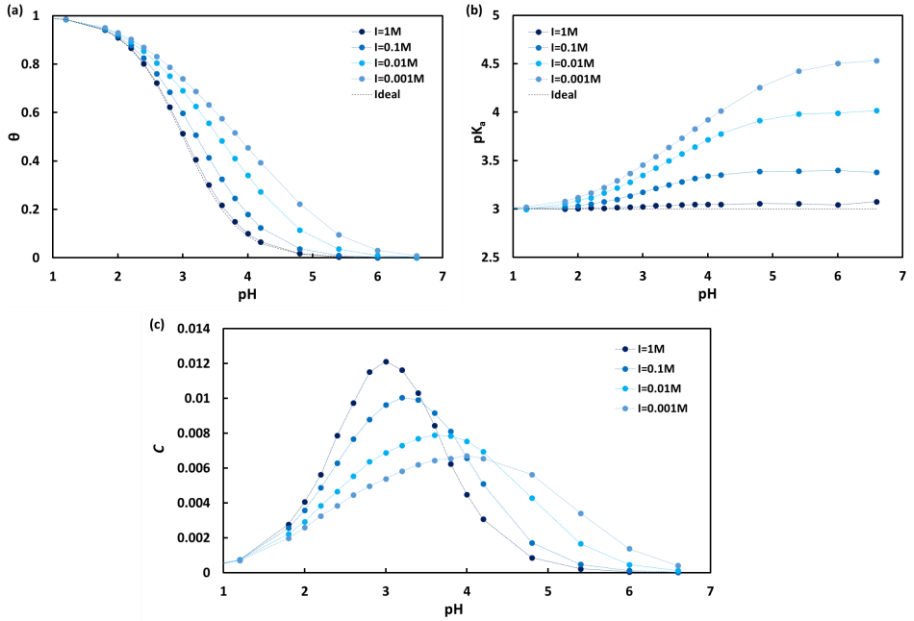

Figure 6. (a) Degree of protonation/Coverage θ; (b) negative logarithm of the effective acidity constant pK_a^{eff} and (c) binding capacity C plotted against pH of a 20-monomer HA chain with ionizable sites of intrinsic pK_a=3.0 in absence of pulling force. Ionic strengths go from 1M (dark blue) to 0.001M (sky blue).

As it can be observed in **Figure 6 (a)**, the degree of protonation is reduced when the ionic strength is increased, due to the shielding that charged sites suffer. When the ionizable sites are not surrounded by a huge number of ions (low ionic strengths), they repel each other increasing the total free energy and the system compensates it reducing the number of charged sites and therefore increasing the coverage (θ) of the macromolecule. Obviously, an increase in the pH also produces a diminishment in the degree of protonation since the HA equilibrium becomes displaced.

The pK_a^{eff} is depicted in **Figure 6 (b)**. At high ionic strengths, the pK_a^{eff} practically coincides with the theoretical intrinsic one for each site of the chain, but when the ionic strength is progressively lowered, the macromolecule appears to be less acidic (pK_a^{eff} rises). This effect can be explained with the same arguments used to justify the θ behaviour since both magnitudes are directly related.

The binding capacity C from **Figure 6 (c)** has the shape of a gaussian distribution. When the ionic force is increased the curve flattens and widens indicating that proton binding

fluctuation is more feasible in a wider range of pH values. Additionally, C maxima appear more displaced to higher pH values since the coverage inflection points are also shifted in the same direction.

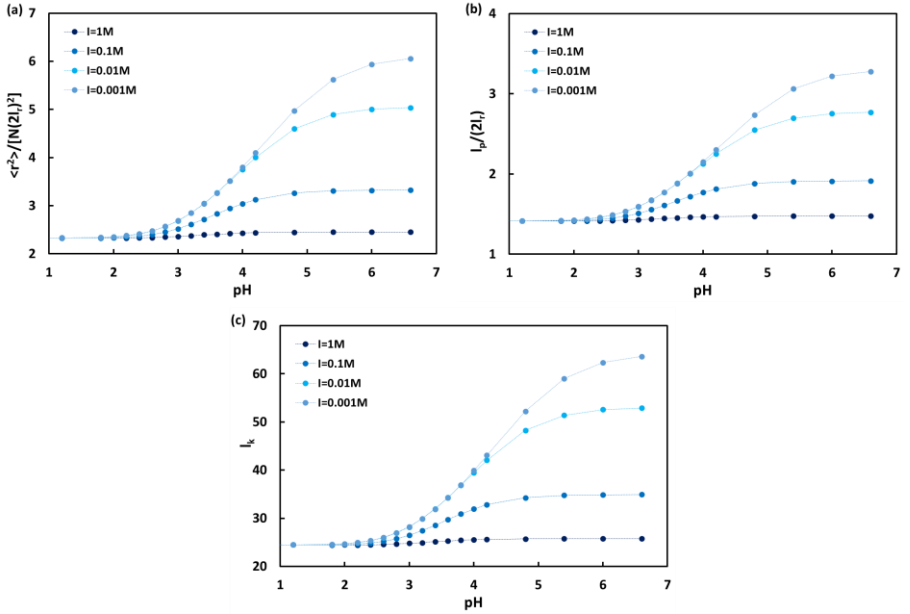

Figure 7. (a) End-to-end distance $\langle r^2 \rangle$; (b) persistence length l_p and (c) Kuhn length l_k plotted against pH of a 20-monomer HA chain with ionizable sites of intrinsic pK_a=3.0 in absence of pulling force. The end-to-end distance is normalized with its expected FJC value $(N(2l_r)^2)$ where $N = 20$ is the number of sites and $l_r = 5.25$ is the average ring distance. The persistence length is normalized to the fully extended monomer length which is established as $2l_r$. Ionic strengths go from 1M (dark blue) to 0.001M (sky blue).

The values of the end-to-end distance $\langle r^2 \rangle$, the persistence length l_p and the Kuhn length l_k are graphed in the charts from **Figure 7**. The figures reveal that when pH is increased and ionic strength is lowered, the HA chain becomes stiffer and larger in order to avoid repulsion among charged sites. For instance, in the most extreme case (pH=6.6 and I=0.001M), the values for these parameters are almost tripled from those at low pH, showcasing how CR affects the spatial configuration of the weak PE.

7.2. STRETCHING EXPERIMENTS

Once the titration curves have been assessed, it is crucial to determine the impact of the mechanical work on the properties of our HA molecule. To evaluate this, L_z ,θ, and l_p are represented against F_z, that is the force exerted in a particular direction which has been assumed as the z-axis. Experiments have been carried out at different pH values (3, 4 and 5) and at different ionic strengths (1M, 0.1M, 0.01M and 0.001M).

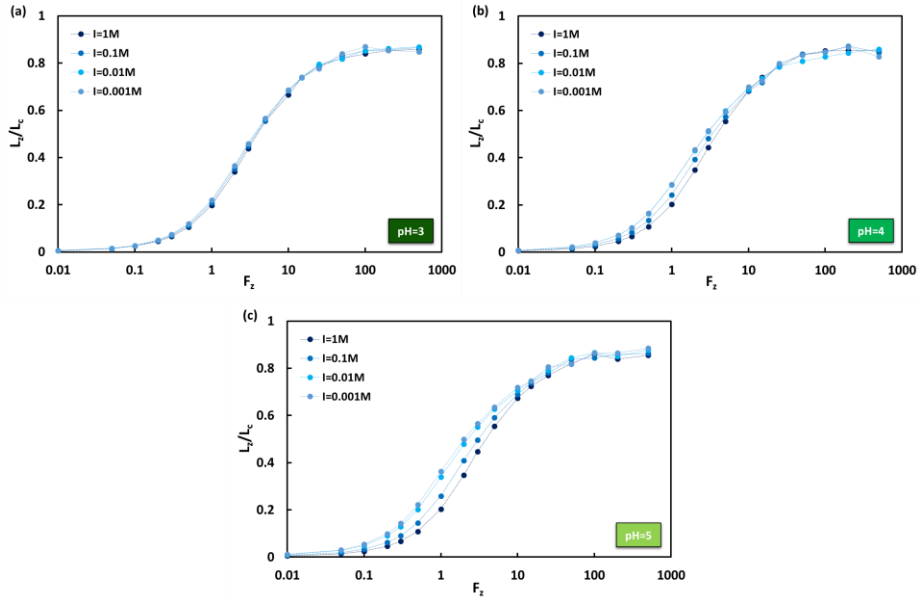

Figure 8. Chain elongation L_z normalized to the contour length $L_c = 2Nl_r$ plotted against the pulling force F_z of a 20-monomer HA chain with ionizable sites of intrinsic pK_a=3.0 at constant pH values equal to (a) 3; (b) 4 and (c) 5. Ionic strengths go from 1M (dark blue) to 0.001M (sky blue).

To begin with, L_z normalized to the contour length of the HA chain is displayed in **Figure 8** grouped at constant pH to discern the ionic strength effect. As it can be seen, when the ionic strength is lowered, L_z increases due to the repulsion among charged sites, thus facilitating the extension of the macromolecule. However, at values greater than 100-200 pN the HA chain is almost equally elongated since the pulling force starts to rule entirely the process, although it is a bit difficult to appreciate that in the charts since the code still struggles with the formation of knots throughout the PE chain when huge forces are applied. On the other hand, in **Figure 9** force-extension curves are depicted at constant ionic strength, and it can be observed that pH

provides a similar outcome; when it is increased, the coverage declines and charge repulsion is intensified, generating a larger extension of the chain until high forces are reached.

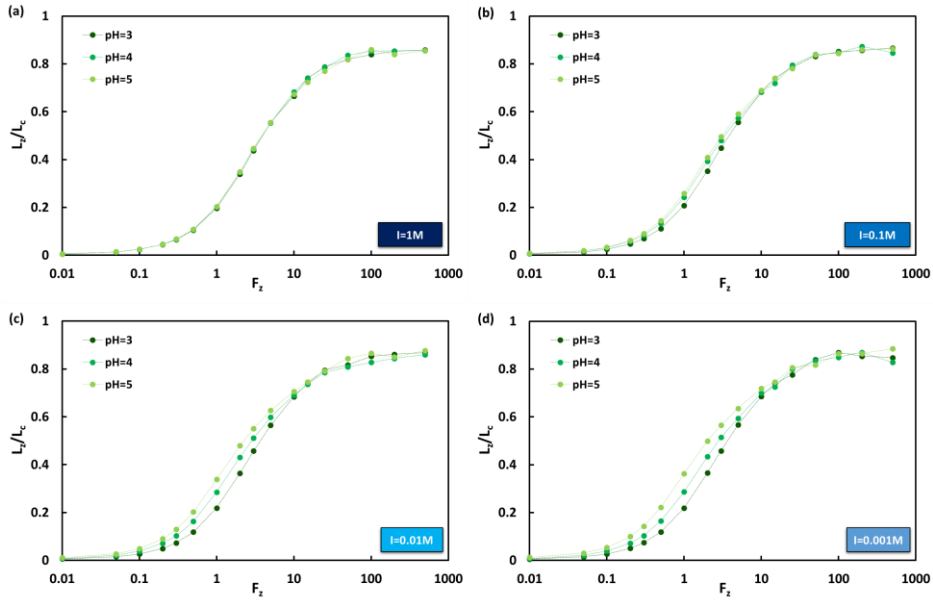

Figure 9. Chain elongation L_z normalized to the contour length $L_c = 2Nl_r$ plotted against the pulling force F_z of a 20-monomer HA chain with ionizable sites of intrinsic pK_a=3.0 at constant ionic strength values equal to (a) 1M; (b) 0.1M; (c) 0.01M and (d) 0.001M. The pH values go from 3 (dark green) to 5 (lawn green).

The degree of protonation θ is represented in **Figure 10**. Its is an important feature since it clearly shows the dependence relationship between the weak PE's charge and the extension force, evincing a CR phenomenon. It can be noted from the graphs that the ionic strength substantially modifies θ, but this also happened when no mechanical force was applied; however, what is important to remark is that at high forces the coverage tends to diminish, reducing thereby the differences among the distinct ionic strengths. This occurs because when the macromolecule is extended, charged sites become more separated and repulsion is lowered, allowing lesser coverage values. The pH influence has not been represented since θ strictly depends on it and the stretching effects go almost unnoticed.

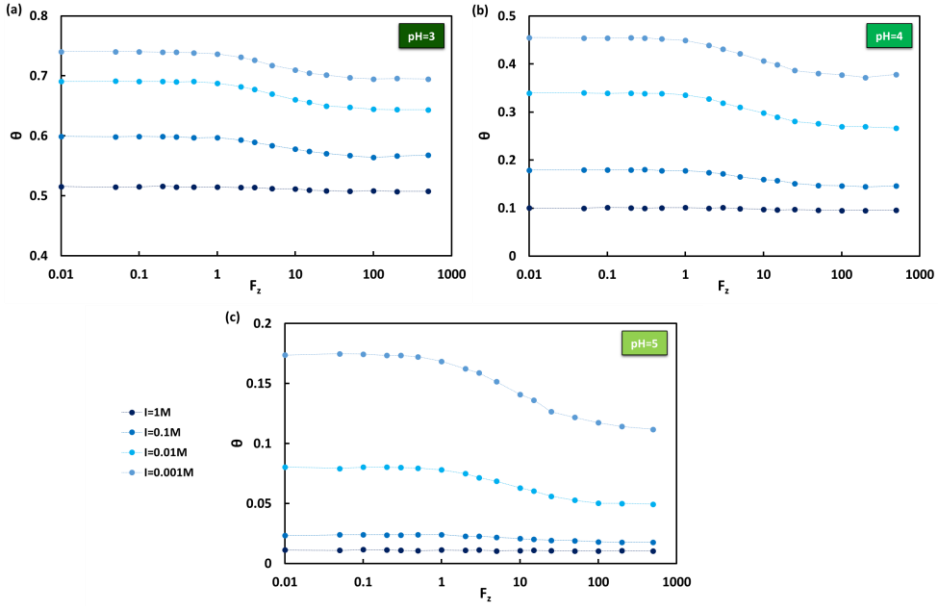

Figure 10. Degree of protonation/Coverage θ plotted against the pulling force F_z of a 20-monomer HA chain with ionizable sites of intrinsic pK_a=3.0 at constant pH values equal to (a) 3; (b) 4 and (c) 5. Ionic strengths go from 1M (dark blue) to 0.001M (sky blue).

With regard to the flexibility of the polymer, the normalised persistence length is pictured in **Figure 11**. From these data it can be ascertained that l_p is virtually constant at pH values higher than 3 and ionic strengths above 1M if little force is applied. When the pH is raised or the ionic strength is lowered, the interaction among charged sites increases (due to either a higher number of deprotonated sites or because the shielding is less effective, respectively) and the HA chain becomes stiffer, since the electrostatic repulsion prevents the macromolecule from folding. Nevertheless, the major cause of l_p variation in these stretching experiments is the pulling force, because it blocks most HA configurations allowing only those that align the chain around the z-axis. This fact makes l_p to achieve normalized values around 8, which indicates that the polymer is correlated for distances up to 8 monomers long.

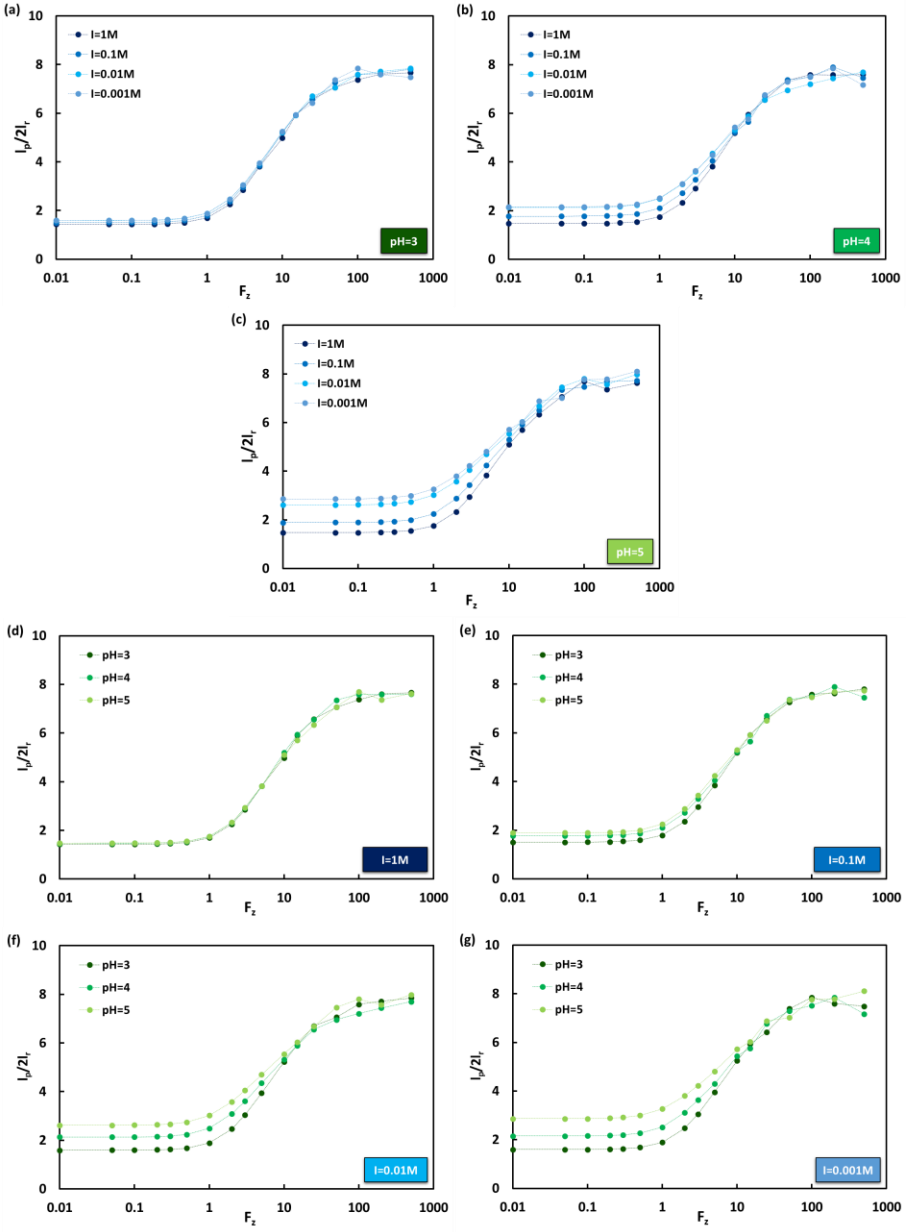

Figure 11. Persistence length l_p normalized to the monomer length ($2l_r$) plotted against the pulling force F_z of a 20-monomer HA chain with ionizable sites of intrinsic pK_a=3.0 at constant pH values equal to (a) 3; (b) 4 and (c) 5 and at constant ionic strength values equal to (d) 1M; (e) 0.1M; (f) 0.01M and (g) 0.001M.

7.3. COMPARISON OF HA-CG4 AND HA-CG9 OUTLINES

In this part, a comparison between HA-CG4 and HA-CG9 outlines is carried out in order to determine if the more sophisticated layout provides significantly better results than the simpler one. To contrast them, simulations results are analysed following a parallel procedure than that used in the preceding sections, where titration curves are examined first and stretching experiments afterwards.

7.3.1. Comparison at zero-force

As it can be observed in **Figure 12**, the outcome for θ and pK_a^{eff} seems to be really similar for both layouts. Only fine disparities are noticeable at the lowest ionic strength (I=0.001M), in which HA-CG9 outline predicts values that are slightly below to those from HA-CG4; and at intermediate ionic strength (I=0.1M), where the trend is the opposite. The lower values for the HA-CG9 layout at I=0.001M could be argued based on the more precise location of the charge that hinders repulsion a little bit but, as the tendencies are not clear, it could also be an effect related to a restriction in the degrees of freedom in the HA-CG4 outline.

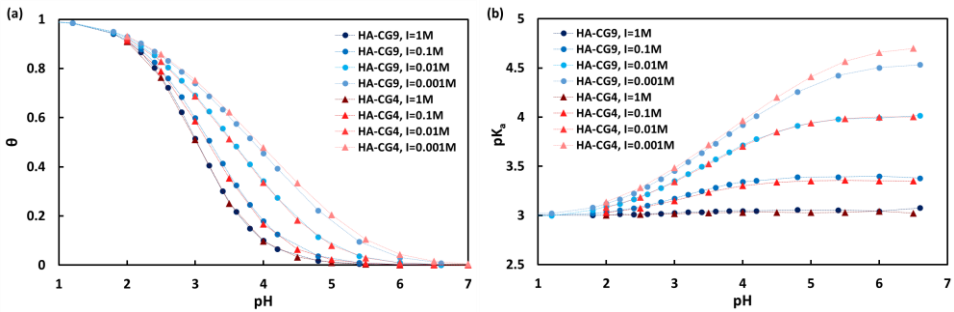

Figure 12. (a) Degree of protonation/Coverage θ and (b) negative logarithm of the effective acidity constant pK_a^{eff} plotted against pH of a 20-monomer HA chain with ionizable sites of intrinsic pK_a=3.0 in absence of pulling force. Red triangles represent the simulations performed with HA-CG4, whereas blue dots represent those performed with HA-CG9. Ionic strengths go from 1M (dark blue/intense red) to 0.001M (sky blue/light red).

7.3.2. Stretching comparison

During all stretching experiments, three distinct force regimes can be discerned comparing both outlines. The first one appears at low forces ($F_z < k_BT/l_p \approx$ 1-2 pN) [47], where the

normalised persistence length can be considered almost constant and the chain behaves as a structureless set of segments of distance l_p [3]. However, at the intermediate-force regime, the HA stretching is mainly controlled by the chain conformational degrees of freedom, which make the macromolecule to adopt internal rotational angles that favour its elongation. Finally, at enough large forces (over 200 pN) the PE lengthening becomes governed by the stretching and bending harmonic potentials, deforming HA bonds and angles, since no more mechanisms allow the stretching of the polymer.

L_z is depicted in **Figure 13** at constant pH or ionic strength depending on the graph. At first sight it may seem that the ionic strength does not affect this magnitude, but this is because the ionic strengths plotted are so low that they can be considered to be equal, and therefore this does not contradict what was asserted in section 7.2. Conversely, the influence of pH can be easily spotted. At low force regimes L_z coincides in both layouts, however, when the force increases, L_z bifurcates acquiring lesser values with HA-CG4 simulations; and this effect is enhanced when pH is raised. This fact is related to the behaviour at intermediate-force regimes; since HA-CG9 has more conformational degrees of freedom, it is more flexible and requires less effort to be extended.

Apart from that, it must be denoted that at high force regimes HA-CG9 stabilizes its L_z value portraying a sigmoidal behaviour whereas HA-CG4 draws a linear increase with the force. This is a direct cause of having achieved the high-force regime, as the stretching and bending constants for the HA-CG9 outline were greater than HA-CG4 to prevent the artificial opening of chemical rings, the PE becomes more rigid with HA-CG9. However, in HA-CG4 this does not happen since its harmonic potentials allow a greater extension until a certain maximum value.

The degree of protonation plotted in **Figure 14** depends strongly on the pH but also on the ionic strength conditions as it has been pointed before, increasing when they are raised or lowered respectively. Nevertheless, what is intriguing of this feature in this stretching experiment is the evolution of θ for each outline when force is applied, more than its own value which is barely the same. In the HA-CG9 outline, θ is constant at low and high force regimes and describes a linear transition at the intermediate range, however, HA-CG4 depicts θ as constant at the beginning (beneath the value for HA-CG9) but then it shows a linear decay for forces greater than 1pN.

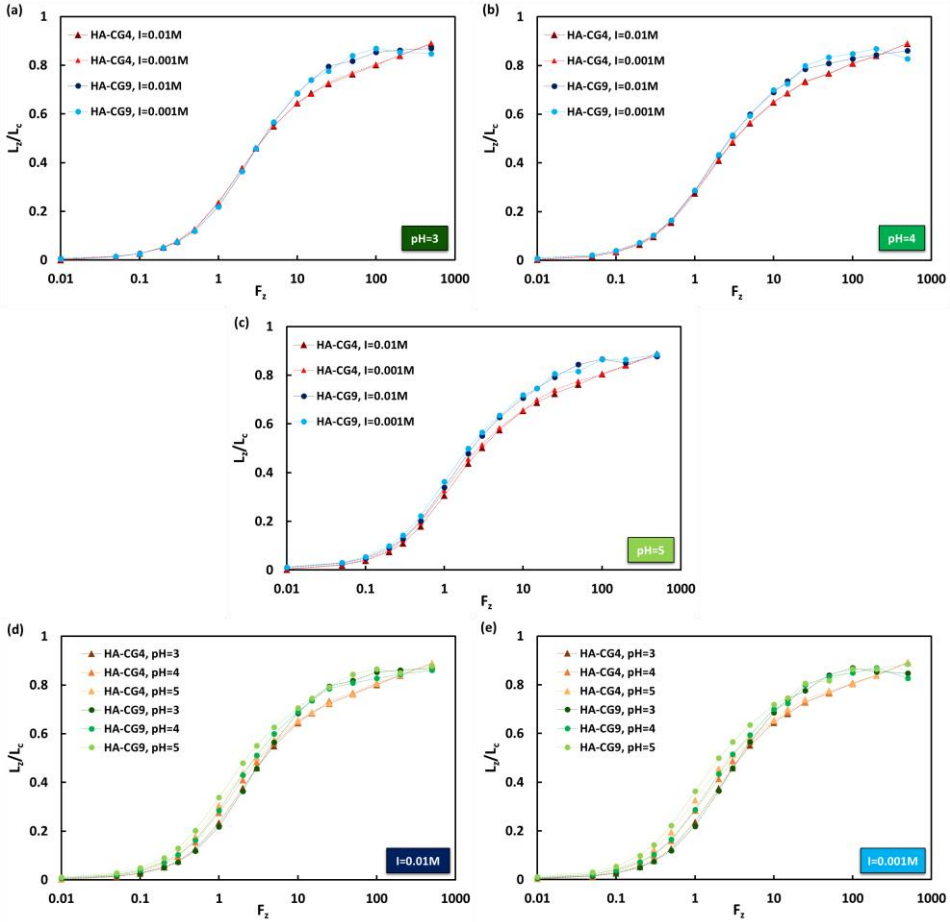

Figure 13. Chain elongation L_z normalized to the contour length $L_c = 2Nl_r$ plotted against the pulling force F_z of a 20-monomer HA chain with ionizable sites of intrinsic pK_a=3.0 at constant pH values equal to (a) 3; (b) 4 and (c) 5; and at constant ionic strength values equal to (d) 0.01M and (e) 0.001M. Triangles represent the simulations performed with HA-CG4, whereas dots represent those performed with HA-CG9.

This can be interpreted with the same reasoning used for L_z. HA-CG9 depicts smaller coverage values at medium forces because its conformational leeway permits more lengthening and therefore more distance among charged sites. Notwithstanding, when high-forces are reached HA-CG4 wins in that regard, because it can be extended further by means of chain deformation showing lower θ values.

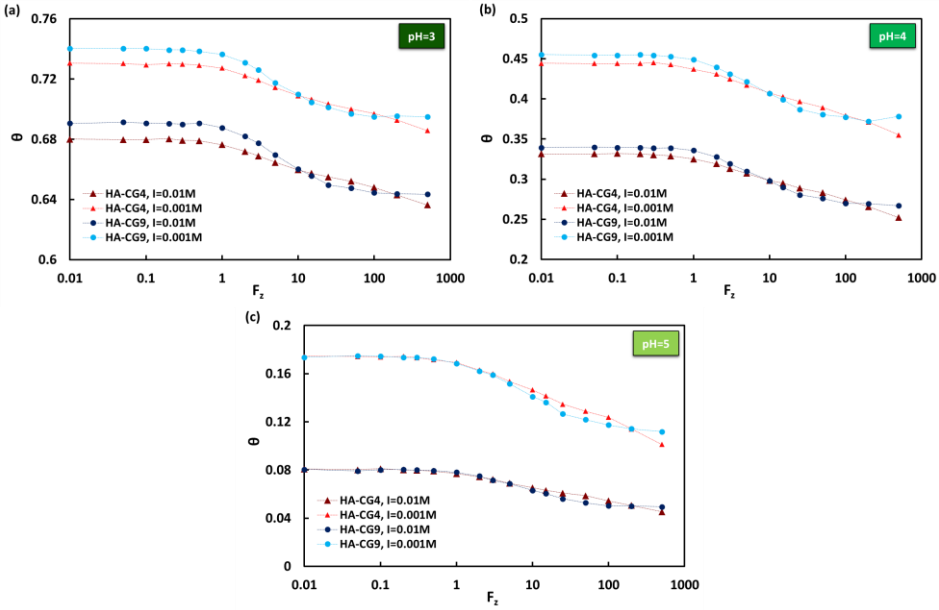

Figure 14. Degree of protonation/Coverage θ plotted against the pulling force F_z of a 20-monomer HA chain with ionizable sites of intrinsic pK_a=3.0 at constant pH values equal to (a) 3; (b) 4 and (c) 5. Red triangles represent the simulations performed with HA-CG4, whereas blue dots represent those performed with HA-CG9.

Eventually, l_p is portrayed in **Figure 15**. At a glance, it can be observed that for both layouts the values for l_p practically coincide for forces under 30-50 pN (except for those at pH=3 that differ a little bit) meaning that the flexibility of the chain is almost the same in this pulling force range. For intermediate forces (between 50-100 pN) where the conformational degrees of freedom are activated, HA-CG9 shows l_p values that are slightly greater than those for HA-CG4, although differences here are not so clear as in the previous examples.

Nonetheless, for values of F_z larger than 100 pN, the macromolecule describes the two expected different behaviours (similarly to what happened with L_z): one more linear for HA-CG4 due to the deformation of the chain, that allows major correlation among the chemical bonds; and another one that ends up roughly in a horizontal asymptote for HA-CG9 since the chain is almost at its maximum extension and cannot be more correlated.

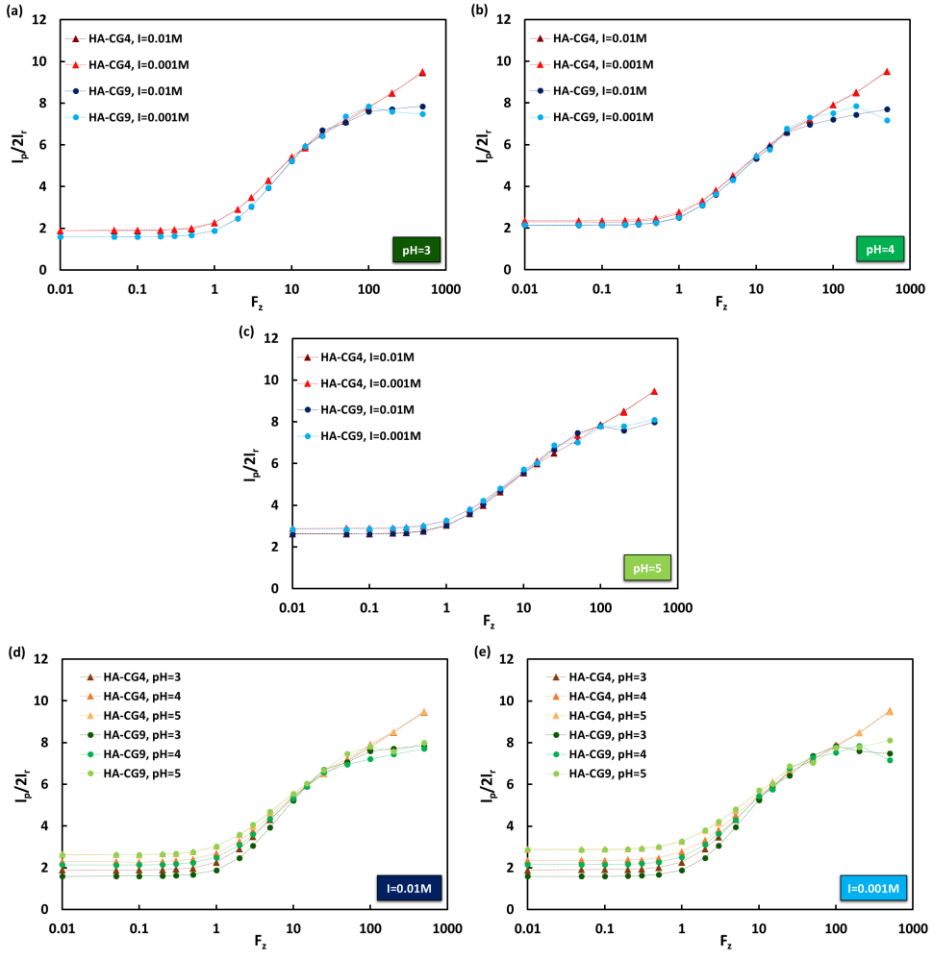

Figure 15. Persistence length l_p normalized to the monomer length ($2l_r$) plotted against the pulling force F_z of a 20-monomer HA chain with ionizable sites of intrinsic pK_a=3.0 at constant pH values equal to (a) 3; (b) 4 and (c) 5; and at constant ionic strength values equal to (d) 0.01M and (e) 0.001M. Triangles represent the simulations performed with HA-CG4, whereas dots represent those performed with HA-CG9.

8. CONCLUSIONS

In the present work, a computational study to determine the effect of charge regulation in the properties of hyaluronic acid was performed. For this purpose, a minimal model that still captures the essentials of weak linear polyelectrolyte stretching (conformational equilibrium, proton binding, bond stretching and bending, steric hinderance and mechanical work) was used to describe the macromolecule. The SBRIS model is its cornerstone, and allows to consider conformational and ionization equilibria, whereas bond stretching and bending are taken into account using harmonic potentials. The electrostatic interactions mediated by the solvent are implemented via the mean field Debye-Hückel potential and steric hinderance is included by means of a hard sphere potential. Finally, the mechanical work can be added to conduct stretching experiments and is calculated as the scalar product between the chain vector and the exerted force.

This minimal model was analysed modifying a Semi-Grand Canonical MonteCarlo code, previously developed by our group, to carry out simulations at constant pH, force and ionic strength; using the parameters from two different coarse-grained outlines that were designed to represent the HA macromolecule. Eventually, assessing the simulations outcome we can draw the subsequent conclusions:

- It is crucial to design the PE layout fitting the linearity requirements but being as accurate as possible to obtain realistic approximations, since the total free energy of the system must encompass all the significant energy contributions and precisely describe them, in order to provide feasible conformations and depict the actual behaviour of the macromolecule.
- Experiments carried out at zero-force show strong dependence on pH and ionic strength conditions. Lowering the ionic strength leads to higher θ and pK_a^{eff} values due to a reduction in the shielding of the ions from the media; since repulsion is intensified, the macromolecule palliates this effect diminishing the number of charged sites. Apart from that, the increase in pH added up to the lowering in the ionic strength produces the chain to rise its overall charge and, consequently, to elongate and

become stiffer (generating an increase in l_p, indicating that correlation extends over longer distances).

- Stretching experiments also show a clear influence of pH and ionic strength, although it becomes less important as force rises. The exertion of the pulling force causes the polyelectrolyte chain to spread along the z direction (which is arbitrary chosen as the force's direction) distancing the ionizable sites. This produces a reduction in the electrostatic repulsion, facilitating the macromolecule deprotonation (decrease in θ), but also increases the rigidity of the polymer, since its conformations are restricted around the z-axis; showing the paradigmatic effect of CR in weak PE.
- In the simulations of force-extension curves, three different force regimes can be discerned. At low forces (less that 1 or 2 pN) the PE stretching is mostly influenced by the pH and ionic strength conditions; at intermediate forces (from 1-2 to 100-200 pN) the elongation of the chain becomes controlled by the conformational degrees of freedom; and finally, at large forces (greater than 200 pN) the stretching events are ruled by the harmonic potentials that portray the deformation of the chain.
- From the comparison between the proposed outlines, it cannot be ensured that the HA-CG9 conducts a better description than the HA-CG4, since none of them have been contrasted with experimental data. However, we know that HA-CG9 is more flexible at the intermediate-force regime since it can be more elongated due to its large number of coarse-grained groups that enhance HA conformations, but is stiffer at high-force regimes as the harmonic potential constants are huge. With HA-CG4 we have the opposite case, it is more rigid at intermediate-force regimes because it has only 4 coarse-grained groups, but it is able to deform at high forces since its stretching and bending constants are smaller.
- An important issue to highlight is the new advancements that are being studied in this field, like the amelioration of current codes to reduce computational costs, the implementation of transfer matrix methods to provide analytic solutions, or the use of all-atom simulations. However, the last two involve complex mathematic and quantum descriptions respectively, a fact that still hampers their development and forces us to work with more classical models despite their limitations.

9. REFERENCES AND NOTES

1. Hassan, P.A.; Verma, G.; Ganguly, R. *Soft materials-properties and applications*; Elsevier Inc., **2012**.
2. Stuart, M.C.; de Vries, R.; Lyklema, H. Polyelectrolytes. *Fundam. Interface Colloid Sci.* **2005**, *5*, 2.1-2.84.
3. Blanco, P.M.; Madurga, S.; Mas, F.; Garcés, J.L. Effect of Charge Regulation and Conformational Equilibria in the Stretching Properties of Weak Polyelectrolytes. *Macromolecules* **2019**, *52*, 8017–8031.
4. Hamacek, J.; Borkovec, M.; Piguet, C. Simple thermodynamics for unravelling sophisticated self-assembly processes. *J. Chem. Soc. Dalt. Trans.* **2006**, *60*, 1473–1490.
5. Rivas, B.L.; Pereira, E.D.; Moreno-Villoslada, I. Water-soluble polymer–metal ion interactions. *Eur. Polym. J.* **2008**, *44*, 2330–2338.
6. Trefalt, G.; Behrens, S.H.; Borkovec, M. Charge Regulation in the Electrical Double Layer: Ion Adsorption and Surface Interactions. *Langmuir* **2016**, *32*, 380–400.
7. Chapel, J.P.; Berret, J.F. Versatile electrostatic assembly of nanoparticles and polyelectrolytes: Coating, clustering and layer-by-layer processes. *Curr. Opin. Colloid Interface Sci.* **2012**, *17*, 97–105.
8. Carnal, F.; Clavier, A.; Stoll, S. Polypeptide-nanoparticle interactions and corona formation investigated by monte carlo simulations. *Polymers (Basel).* **2016**, *8*.
9. Meyer, K.; Palmer, J.W. Polysaccharide of Vitreous Humor. *J. Biol. Chem.* **1934**, *107*, 629–634.
10. Hascall, V.C.; Majors, A.K.; De La Motte, C.A.; Evanko, S.P.; Wang, A.; Drazba, J.A.; Strong, S.A.; Wight, T.N. Intracellular hyaluronan: A new frontier for inflammation? *Biochim. Biophys. Acta - Gen. Subj.* **2004**, *1673*, 3–12.
11. Toole, B.P. Hyaluronan: From extracellular glue to pericellular cue. *Nat. Rev. Cancer* **2004**, *4*, 528–539.
12. Cleland, R.L.; Wang, J.L.; Detweiler, D.M.; Wang, J.L. Polyelectrolyte Properties of Sodium Hyaluronate, 2. Potentiometric Titration of Hyaluronic Acid. *Macromolecules* **1982**, *15*.
13. Cowman, M.K.; Matsuoka, S. Experimental approaches to hyaluronan structure. *Carbohydr. Res.* **2005**, *340*, 791–809.
14. Turley, E.A.; Noble, P.W.; Bourguignon, L.Y.W. Signaling properties of hyaluronan receptors. *J. Biol. Chem.* **2002**, *277*, 4589–4592.

15. Toole, B.P. Hyaluronan in morphogenesis. *Semin. Cell Dev. Biol.* **2001**, *12*, 79–87.
16. Wu, X.; Cao, L.; Li, F.; Ma, C.; Liu, G.; Wang, Q. Hyaluronic acid hydrogel in the treatment of osteoarthritis. *Am. J. Transl. Res.* **2018**, *10*, 1143–1154.
17. Goa, K.L.; Benfield, P. Hyaluronic Acid: A Review of its Pharmacology and Use as a Surgical Aid in Ophthalmology, and its Therapeutic Potential in Joint Disease and Wound Healing. *Drugs* **1994**, *47*, 536–566.
18. Brown, M.B.; Jones, S.A. Hyaluronic acid: A unique topical vehicle for the localized delivery of drugs to the skin. *J. Eur. Acad. Dermatology Venereol.* **2005**, *19*, 308–318.
19. Giannotti, M.I.; Vancso, G.J. Interrogation of single synthetic polymer chains and polysaccharides by AFM-based force spectroscopy. *ChemPhysChem* **2007**, *8*, 2290–2307.
20. Smith, S.B.; Finzi, L.; Bustamante, C. Mechanical Measurements of the Elasticity of Single DNA Molecules by Using Magnetic Beads; *Science* **1992**, *258*, 1122–1126, doi:10.1126/science.1439819.
21. Frielinghaus, H. *C1 Flexible Polymers*; **2004**.
22. Glatting, G.; Winkler, R.G.; Reineker, P. Partition Function and Force Extension Relation for a Generalized Freely Jointed Chain. *Macromolecules* **1993**, *26*, 6085–6091.
23. Radiom, M.; Borkovec, M. Influence of ligand-receptor interactions on force-extension behavior within the freely jointed chain model. *Phys. Rev. E* **2017**, *96*, 1–7.
24. Giannotti, M.I.; Rinaudo, M.; Vancso, G.J. Force spectroscopy of hyaluronan by atomic force microscopy: From hydrogen-bonded networks toward single-chain behavior. *Biomacromolecules* **2007**, *8*, 2648–2652.
25. Kratky, O.; Porod, G. Röntgenuntersuchung gelöster Fadenmoleküle. *Recl. des Trav. Chim. des Pays-Bas* **1949**, *68*, 1106–1122.
26. Doi, M.; Edwards, S. *The theory of polymer dynamics*; Oxford University Press: New York; **1990**.
27. Milstein, J.N.; Meiners, J.; Arbor, A. Encyclopedia of Biophysics. *Encycl. Biophys.* **2013**.
28. Marko, J.F.; Siggia, E.D. Stretching DNA. *Macromolecules* **1995**, *28*, 8759–8770.
29. Bustamante, C.; Bryant, Z.; Smith, S.B. mechanics. **2003**, *421*.
30. Neuman, K.C.; Nagy, A. Single-molecule force spectroscopy: Optical tweezers, magnetic tweezers and atomic force microscopy. *Nat. Methods* **2008**, *5*, 491–505.
31. Katiyar, R.S.; Jha, P.K. Phase behavior of aqueous polyacrylic acid solutions using atomistic molecular dynamics simulations of model oligomers. *Polymer (Guildf).* **2017**, *114*, 266–276.
32. Borkovec, M.; Koper, G.J.M.; Jönsson, B. ; In *Surface and Colloid Science*; Matigeric, E., Ed.; Plenum Press: New York, USA, **2001**; pp. 99–339.

33. Flory, P.J. Foundations of Rotational Isomeric State Theory and General Methods for Generating Configurational Averages. *Macromolecules* **1974**, *7*, 381–392.
34. Livadaru, L.; Kreuzer, H.J. Statistical mechanics of an n-alkane chain in θ-condition: Going beyond the RIS model. *Phys. Chem. Chem. Phys.* **2004**, *6*, 3872–3878.
35. Garcés, J.L.; Madurga, S.; Borkovec, M. Coupling of conformational and ionization equilibria in linear poly(ethylenimine): A study based on the site binding/rotational isomeric state (SBRIS) model. *Phys. Chem. Chem. Phys.* **2014**, *16*, 4626–4638.
36. Blanco, P.M.; Madurga, S.; Narambuena, C.F.; Mas, F.; Garcés, J.L. Role of charge regulation and fluctuations in the conformational and mechanical properties ofweak flexible polyelectrolytes. *Polymers (Basel).* **2019**, *11*.
37. Garcés, J.L.; Madurga, S.; Rey-Castro, C.; Mas, F. Dealing with long-range interactions in the determination of polyelectrolyte ionization properties. Extension of the transfer matrix formalism to the full range of ionic strengths. *J. Polym. Sci. Part B Polym. Phys.* **2017**, *55*, 275–284.
38. Koper, G.J.M.; Borkovec, M. Proton binding by linear, branched, and hyperbranched polyelectrolytes. *Polymer (Guildf).* **2010**, *51*, 5649–5662.
39. Blanco, P.M.; Madurga, S.; Mas, F.; Garcés, J.L. Coupling of charge regulation and conformational equilibria in linearweak polyelectrolytes: Treatment of long-range interactions via effective short-ranged and pH-dependent interaction parameters. *Polymers (Basel).* **2018**, *10*.
40. Sodric, S. Stretching of weak polyelectrolytes at the single-molecule level, Bachelor Thesis; Universitat de Barcelona, **2019**.
41. Metropolis, N.; Rosenbluth, A.W.; Rosenbluth, M.N.; Teller, A.H.; Teller, E. Equation of state calculations by fast computing machines. *J. Chem. Phys.* **1953**, *21*, 1087–1092.
42. Gelman, A.; Roberts, G.O.; Gilks, W.R. Efficient Metropolis jumping rules. *Bayesian Stat.* **1996**, *5*, 599–608.
43. Roberts, G.O.; Gelman, A.; Gilks, W.R. Weak convergence and optimal scaling of random walk Metropolis algorithms. *Ann. Appl. Probab.* **1997**, *7*, 110–120.
44. Lund, M.; Jönsson, B. Charge regulation in biomolecular solution. *Q. Rev. Biophys.* **2013**, *46*, 265–281.
45. Hans, K.; Försterling, H.-D.; Waldeck, D. *Principles of Physical Chemistry*; Second Edi.; Wiley: New Jersey, **2009**.
46. Lamour, G.; Kirkegaard, J.B.; Li, H.; Knowles, T.P.J.; Gsponer, J. Easyworm: An open-source software tool to determine the mechanical properties of worm-like chains. *Source Code Biol. Med.* **2014**, *9*, 1–6.
47. Livadaru, L.; Netz, R.R.; Kreuzer, H.J. Stretching response of discrete semiflexible polymers. *Macromolecules* **2003**, *36*, 3732–3744.

10. ACRONYMS

AFM: Atomic Force Microscopy

CR: Charge Regulation

DH: Debye-Hückel

EV: Excluded Volume

FJC: Freely Jointed Chain

HA: Hyaluronic Acid

MC: MonteCarlo

NSI: Non-Specific Interactions

PE: Polyelectrolyte

RIS: Rotational Isomeric State

SB: Site Binding

SBRIS: Site Binding Rotational Isomeric State

SGCMC: Semi-Grand Canonical Monte Carlo

SI: Specific Interactions

SMFS: Single-Molecule Force Spectroscopy

WLC: Worm Like Chain